


ORIGINAL ARTICLE

Influence of the biomechanical evaluation of rupture using two shapes of same intramedullary implant after proximal interphalangeal joint arthrodesis to correct the claw/hammer pathology: A finite element study

Javier Bayod-López¹ | Ricardo Becerro-de-Bengoa-Vallejo² |
Juan Carlos Prados-Frutos³ | Marta Losa-Iglesias⁴ | Daniel López-López⁵  |
María Prados-Privado⁶

¹Applied Mechanics and Bioengineering Group (AMB), Aragon Institute of Engineering Research (I3A), Centro de Investigación Biomédica en Red CIBER-BBN, Spain, Universidad de Zaragoza, Zaragoza, Spain

²Facultad de Enfermería, Fisioterapia y Podología, Universidad Complutense de Madrid, Madrid, Spain

³Department of Medical Specialties and Public Health, IDIBO Group (High Performance Group in Research and Development of Biomaterials in Dentistry), Rey Juan Carlos University, Madrid, Spain

⁴Facultad de CC de la Salud, Universidad Rey Juan Carlos, Madrid, Spain

⁵Research, Health and Podiatry Group, Department of Health Sciences, Faculty of Nursing and Podiatry, Industrial Campus of Ferrol, Universidade da Coruña, Ferrol, Spain

⁶Department Continuum Mechanics and Structural Analysis, Higher Polytechnic School, Carlos III University, Leganes, Madrid, Spain

Correspondence

Daniel López-López, Research, Health and Podiatry Group, Department of Health Sciences, Faculty of Nursing and Podiatry, Industrial Campus of Ferrol, Universidade da Coruña, Ferrol, Spain.
Email: daniellopez@udc.es

Funding information

Economy and Competitiveness Ministry, Grant/Award Number: DPI2013-44987-R; Funding for open access charge: Universidade da Coruña/CISUG.

Abstract

We used finite element analysis to study the mechanical stress distribution of a new intramedullary implant used for proximal interphalangeal joint (PIPJ) arthrodesis (PIPJA) to surgically correct the claw-hammer toe deformity that affects 20% of the population. After geometric reconstruction of the foot skeleton from claw toe images of a 36-year-old male patient, two implants were positioned, in the virtual model, one neutral implant (NI) and another one 10° angled (10°AI) within the PIPJ of the second through fourth HT during the toe-off phase of gait and results were compared to those derived for the non-surgical foot (NSF). A PIPJA was performed on the second toe using a NI reduced tensile stress at the proximal phalanx (PP) (45.83 MPa) compared to the NSF (59.44 MPa; $p < 0.001$). When using the 10°AI, the tensile stress was much higher at PP and middle phalanges (MP) of the same toe, measuring 147.58 and 160.58 MPa, respectively, versus 59.44 and 74.95 MPa at corresponding joints in the NSF (all $p < 0.001$). Similar results were found for compressive stresses. The NI reduced compressive stress at the second PP (−65.12 MPa) compared to the NSF (−113.23 MPa) and the 10°AI (−142 MPa) (all $p < 0.001$). The von Mises stresses within the implant were also

This is an open access article under the terms of the [Creative Commons Attribution-NonCommercial](https://creativecommons.org/licenses/by-nc/4.0/) License, which permits use, distribution and reproduction in any medium, provided the original work is properly cited and is not used for commercial purposes.

© 2024 The Author(s). *International Wound Journal* published by Medicalhelplines.com Inc and John Wiley & Sons Ltd.

significantly lower when using NI versus 10°AI ($p < 0.001$). Therefore, we do not recommend performing a PIPJA using the 10°AI due to the increase in stress concentration primarily at the second PP and MP, which could promote implant breakage.

KEYWORDS

foot, foot deformities, foot diseases, musculoskeletal diseases

Key Messages

- We assessed the mechanical stress distribution of a new intramedullary implant in the toe deformity.
- The shape of 10°AI produces stress concentration around the angularity.
- We do not recommend performing a proximal interphalangeal joint arthrodesis using the 10°AI as it could promote implant breakage.

1 | INTRODUCTION

The prevalence of symptomatic claw toe (CT) and hammer toe (HT) in the literature is reported to be 20% of the population, primarily affecting older adults and individuals with certain risk factors. These risk factors include intrinsic factors (such as age, sex, foot structure, and muscle imbalances) and extrinsic factors (such as footwear, trauma, medical conditions, lifestyle, and work activity).¹⁻³ Surgery for these deformities is among the most commonly conducted interventions in general orthopaedic practice.⁴ CT deformity is characterized by dorsiflexion of the metatarsophalangeal joint (MTPJ), plantar flexion of the proximal interphalangeal joint (PIPJ) and plantar flexion of the distal interphalangeal joint (DIPJ). HT deformity is characterized by dorsiflexion of the MTPJ, plantar flexion of the PIPJ and dorsiflexion of the DIPJ.⁵

Clinically, MTPJ dorsiflexion causes dorsal displacement of the proximal phalanx (PP), driving the head of the PP against the internal surface of the footwear, thereby exerting excessive pressure on the phalangeal head.⁶

The surgical technique used to reduce HT is known as arthrodesis or PIPJ fusion.⁷⁻⁹ According to Monson et al.³⁰ and Schlefman et al.¹⁰ end-to-end arthrodesis is the most common procedure for digital arthrodesis and is most frequently performed on the second digit in middle-aged women.^{5,7,8,10-12}

A variety of fixation techniques are available for performing arthrodesis of the PIPJ as part of HT correction,¹³⁻²⁰ including intramedullary implants which offer a reasonable alternative to the traditional pin stabilization method.

A new intramedullary implant (FDA K070598) consists of a small shape memory titanium alloy anchor

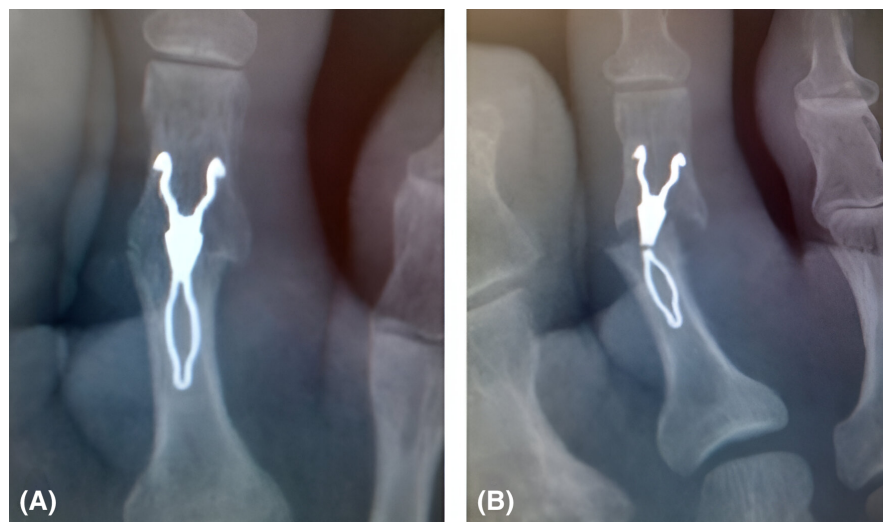
which expands at body temperature. Use of this new intramedullary implant could increase fusion rate, decrease complications and improve patient comfort.²¹

The operative technique using the new shape memory intramedullary implant for arthrodesis of the PIPJ consists of opening the PIPJ through a transverse incision and inserting the implant in a cold (frozen) state which then quickly expands at body temperature, allowing solid fixation within the bones of the proximal and middle phalanges. Delmi performed a prospective study of 170 HT corrections using this new shape memory alloy intramedullary implant for arthrodesis of the PIPJ and reported rupture of only three implants.²² In contrast, only one implant fractured and had to be removed (Figure 1), based on our experience.

Until now, the choice of implant, either neutral implant (NI) or 10° angled implant (10°AI) for PIPJ arthrodesis (PIPJA), was based on the clinical situation, the surgeon's experience and the desired result.²³ However, finite element (FE) modelling is an excellent alternative for evaluating the biomechanical performance of an implant in the foot²⁴⁻²⁷ and for determining displacements and stress levels.^{28,29} In a previous work,³⁰ the advantages and drawbacks of two types of tendon transfer to correct the HT deformity using FE modelling were analysed.

The present study used FE analysis to assess the biomechanical efficacy of PIPJA using 10°AI versus NI shape memory intramedullary implants. In particular, we determined whether these two types of implants could reduce tensile or compressive stresses at the PP and middle phalanx (MP) of the second through fourth toes to reduce the risk of pain or fracture at any phalanx. We did not investigate the fifth toe in the current study as we could not find any evidence in the literature for the use of these implants in the fifth toe.

FIGURE 1 Neutral memory alloy intramedullary implant. (A) For proximal interphalangeal joint arthrodesis (PIPJA), the implant is inserted between proximal and middle phalanges of the second toe. (B) Same implant fractured at 4 weeks after surgery.



The aim of this study was to assess whether there is an increased risk of rupture or implant failure when using the NI implant compared to the 10° AI implant for treating hammer toe (HT) through proximal interphalangeal joint arthrodesis (PIPJA). Based on our clinical experience from previous studies, we compared the biomechanical outcomes of flexor digitorum longus and flexor digitorum brevis tendon transfers for treating claw and hammer toe deformities using finite element simulation,^{30,31} we hypothesized that PIPJA surgery using a NI versus 10° AI would result in the same distribution of tensile and compressive stresses at the proximal and middle phalanx of the toes with equal risk for implant rupture.

2 | MATERIALS AND METHODS

2.1 | Geometry and mesh reconstruction

Institutional review board approval for the study was obtained from the Research Committee of Complutense University. Written informed consent was obtained from our patient according to the guidelines of our institutional review board prior to the start of our experiment.

A total of 93 tomographic images of the feet of a 36-year-old male patient, 60 kg weight, 165 cm height were obtained using a multislice CT (General Electric Waukesha, WI, USA). After geometric reconstruction of the feet from CT images, the intramedullary implant (FDA K070598) was positioned, in the virtual model, at NI and 10° AI within the PIPJ of the second through fourth HT of the patient during the toe-off phase of gait. The results obtained were compared to those derived from the non-surgical foot (NSF) using FE analysis.

The images were segmented with software from the Advanced Computer Science Group of the University of Zaragoza, Spain, through semiautomatically defined splines, which distinguished between cortical and spongy bone. This process was used to reproduce the 28 bones that comprise the foot including the talus, calcaneus, cuboid, navicular, three cuneiforms, five metatarsals, five PPs, four MPs, five DPs and two sesamoid bones. The mesh for each bone was constructed using the Harpoon commercial software program (Harpoon r1.4.5, CEI, Apex, NC, USA), which also distinguished between cortical and spongy bone.

Bones were connected by means of cartilaginous joints while ligaments were modelled using a set of 483 non-compressible one-dimensional elements. A more detailed description of this FE model may be found in García-Aznar et al. and García-Gonzalez et al.^{29,30}

The manufacturer provided two types of implants, NI and 10° AI, available in various dimensions and made from Nitinol. USA, a Memometal Technologies Company, 6060 Poplar Ave., Suite 254, Memphis, TN 38119).

The two implants were scanned in three dimensions to obtain their geometry. These geometries were meshed and introduced into the FE model of the proximal and middle phalanges of the second through fourth toes. For research purposes, the implants placed in the second through fourth toes were STO-19 for the NI and STO-19 for the 10° AI. In the fourth phalanges, smaller implants were used, that is, STO-16 for NI and STO-16 for 10° AI.

At the 'so-called' heel-off and toe-off stages of gait, all of the body's weight falls over the area of the forefoot and the plantar flexor muscles [comprised of the flexor digitorum longus (FDL) and flexor digitorum brevis (FDB) muscles]. Together with the interosseous and lumbrical muscles, the FDL and FDB muscles must maintain the PP in contact with the ground, without producing digital

deformity, in order to maintain balance during walking. The long and short flexors, which contribute to these phases of gait, were modelled with bar elements that were subject to an initial stress of +2% to simulate the tension to which they are subjected during the previously mentioned phases of human gait.³⁰ Moreover, our model does not take into account the interosseous and lumbrical muscles because its function is abolished in the HT deformity.³² The anatomical model consisted of 951 608 linear tetrahedrons for the NI and 981 338 for the angular implant with an average size of 1 mm in both cases. The average size of 1 mm was an optimal choice from the point of view of accuracy and computational cost based on a mesh sensitivity analysis.^{29,33} These two models were exported to the commercial software package ABAQUS (ABAQUS 6.11.3, HKS, Providence, RI, USA), which was used to perform all simulations.

2.2 | Material properties

The bone tissue was modelled by differentiating cortical from spongy bone, and both types of bone were considered elastic and isotropic. The Young's modulus for cortical bone was 17.00 MPa and the Poisson coefficient for cortical bone was 0.3, while the Young's modulus and Poisson coefficient for spongy bone were 700 MPa and 0.3, respectively.³⁴ The cartilage was also considered an elastic and isotropic material, with a Young's modulus of 10 MPa and a Poisson coefficient of 0.4.²⁶

Two groups of ligaments were distinguished based on rigidity, including a more rigid group (plantar fascia, and superficial and deep plantar ligaments) with a Young's modulus of 350 MPa, a Poisson coefficient of 0.3 and a cross-sectional area of 290.7 mm²; and another less rigid group composed of the remaining ligaments, with a Young's modulus of 260 MPa, a Poisson coefficient of 0.3 and a cross-sectional area of 18.4 mm².²⁵ The flexor tendons were also modelled as linear, elastic and incompressible elements, with a Young's modulus of 450 MPa, a Poisson coefficient of 0.3 and a cross-sectional area of 12.5 mm².^{29,35} Finally, implants were modelled as linear and elastic materials with Young's modulus of 110 000 MPa, Poisson coefficient of 0.33 and tensile yield strength of 430 MPa.^{36,37}

2.3 | Loads and boundary conditions

Defining the position of the model is very important, as loads applied to the foot change in both direction and value with each position at the point of application and it seems that the FE analysis method is the best way to determine the mechanical responses of biological systems

under complex loading circumstances.³⁸ With this aim, Geffen et al. proposed dividing the stance phase of the human gait cycle into six phases: initial-contact, heel-strike, midstance, forefoot-contact, push-off and toe-off,²⁷ and latest research has utilized this model FE analysis to evaluate the effect of minimalist footwear running in hallux valgus patients and to understand the biomechanical characteristics of osteoporotic scoliosis.^{39,40}

In the present work, the push-off phase was reproduced. Consequently, we considered the Achilles tendon insertion as a fixed support, as the Achilles tendon is one of the tendons that mechanically generates most of the reactive force countering the load of the body weight. In the push-off phase, the foot is at 85% of the stance phase.²⁶ To simulate this position, the flexors were subjected to an initial tension of 2%. In addition, applying data from the literature^{26,41–43} to a patient with a mass of 60 kg, a load value of 180.5 kg was established, divided into 180 kg of normal force (Fn) at the joint surface and 12 kg of tangential component of force (Ft) to this surface. The joint surface mentioned was that formed by the contact of the tibia and the fibula with the talus. More detailed information concerning loads and boundary conditions can be found in García-González et al.³⁰

2.4 | Analysed cases

We analysed two different surgical solutions for HT: a PIPJA on the second through fourth toes using a NI versus a PIPJA on the second through fourth toes using a 10°AI. Both cases reproduced only the push-off phase of gait.

2.5 | Statistical analysis

The paired Student's t-test was used to determine whether there were significant differences between tensile versus compressive stresses at proximal and middle phalanges of the second through fourth toes when using a NI or 10°AI compared to the NSF model, which was used as the control. The von Mises stress, using NI and 10°AI, was also assessed. In all of the analyses, a *p* value <0.01 (with a 99% confidence interval) was considered statistically significant. All data analyses were conducted using SPSS software, version 14.0 (SPSS Science, Chicago, IL, USA).

3 | RESULTS

Maximum tensile and compressive stresses (Tables 1 and 2, respectively) on the proximal and middle phalanges

TABLE 1 Maximum tensile stress on the proximal and middle phalanges of the non-surgical foot versus after proximal interphalangeal joint arthrodesis using two types of implants (neutral vs. angled). *p* value between NI versus NSF, 10° versus NSF and 10° versus NI are <0.001.

Phalanx (<i>N</i>)	Maximum tensile stress (MPa) average ± SD (minimum –maximum)		
	NSF	NI	10°
2nd PP (<i>n</i> = 20 606)	59.44 (1.83 ± 7.41)	45.83 (1.54 ± 5.21)	147.58 (3.63 ± 14.20)
2nd MP (<i>n</i> = 12 374)	74.95 (1.59 ± 4.35)	94.83 (1.90 ± 3.41)	160.58 (3.54 ± 11.39)
3rd PP (<i>n</i> = 18 574)	77.16 (2.76 ± 10.35)	138.51 (3.62 ± 14.91)	154.08 (4.28 ± 16.81)
3rd MP (<i>n</i> = 10 519)	58.03 (1.34 ± 4.11)	119.77 (3.28 ± 10.73)	174.06 (3.96 ± 12.10)
4th PP (<i>n</i> = 16 573)	50.05 (0.06 ± 0.39)	35.05 (0.65 ± 2.23)	61.59 (1.32 ± 4.44)
4th MP (<i>n</i> = 9310)	43.30 (0.93 ± 2.78)	150.44 (1.22 ± 4.33)	250.01 (2.31 ± 7.72)

Note: *p* < 0.01 (with a 99% confidence interval) was considered statistically significant.

Abbreviations: 10°, 10° angled implant; MP, middle phalanx; MPa, megapascal; *N*, total osseous surface represented by the total number of nodes that make up the cortical and spongy mesh; NI, neutral implant; NSF, non-surgical foot; PIPJA, proximal interphalangeal joint arthrodesis; PP, proximal phalanx.

TABLE 2 Maximum compressive stress on the proximal and middle phalanges of the non-surgical foot versus after proximal interphalangeal joint arthrodesis using two types of implants (neutral vs. angled). *p* value between NI versus NSF, 10° versus NSF and 10° versus NI are <0.001.

Phalanx (<i>N</i>)	Maximum compressive stress (MPa) average ± SD (minimum –maximum)		
	NSF	NI	10°
2nd PP (<i>n</i> = 20 606)	–113.23 (–4.80 ± 14.99)	–65.12 (–2.42 ± 7.58)	–142 (3.77 ± 14.41)
2nd MP (<i>n</i> = 12 374)	–202 (–3.49 ± 9.09)	–104.85 (–1.60 ± 5.11)	–179.19 (–3.21 ± 10.13)
3rd PP (<i>n</i> = 18 574)	–199 (–8.30 ± 24.06)	–152 (–5.18 ± 18.30)	–140 (–5.35 ± 17.89)
3rd MP (<i>n</i> = 10 519)	–308.82 (–6.07 ± 15.99)	–167.01 (–3.88 ± 12.86)	–208.33 (–4.53 ± 13.74)
4th PP (<i>n</i> = 16 573)	–32.08 (–1.93 ± 4.72)	–18.85 (–0.59 ± 1.93)	–39.90 (–1.14 ± 3.81)
4th MP (<i>n</i> = 9310)	–147.39 (–3.07 ± 8.24)	–146.44 (–1.34 ± 4.42)	–288.88 (–2.62 ± 8.52)

Note: *p* value between NI versus NSF, 10° versus NSF and 10° versus NI are <0.001. *p* < 0.01 (with a 99% confidence interval) was considered statistically significant.

Abbreviations: 10°, 10° angled implant; MP, middle phalanx; MPa, megapascal; *N*, total osseous surface represented by the total number of nodes that make up the cortical and spongy mesh; NI, neutral implant; NSF, non-surgical foot; PIPJA, proximal interphalangeal joint arthrodesis; PP, proximal phalanx.

of the second through fourth toes of the NSF were compared to their values after PIPJA for the same toes/phalanges. Tensile stresses were measured along the dorsal aspect and compressive stresses along the plantar aspect of the NSF, and after PIPJA, for the two implant types.

At the second PP joint, the NI reduced tensile stress (45.83 MPa) compared to the NSF (59.44 MPa), however, the 10°AI increased the tensile stress (147.58 MPa; all *p* values <0.001; Table 1). At the second MP joint, the NI and 10°AI significantly increased the tensile stress (94.83 MPa and 160.58 MPa, respectively) compared to the NSF (74.95 MPa) (all *p* values <0.001; Table 1).

Similar findings were noted at the third toe. At both proximal and middle phalanges, the NSF demonstrated less than half the tensile stress exhibited at the third toe using either implant (all *p* values <0.001; Table 1).

At the fourth PP, the NI also reduced tensile stress (35.05 MPa) compared to the NSF (50.05 MPa), however,

the 10°AI increased the tensile stress (61.59 MPa) (all *p* values <0.001; Table 1). At the fourth MP, the opposite was true. The NI and 10°AI significantly increased the tensile stress (150.44 MPa and 250.01 MPa, respectively) compared to the NSF (43.30 MPa; all *p* values <0.001; Table 1).

Similar results were found regarding compressive stresses (Table 2). At the PP of the second toe, the NI reduced compressive stresses at the PP to a maximum value of –65.12 MPa compared with NSF value of –113.23 MPa (*p* < 0.001; Table 2). When using the 10°AI, however, the resulting compressive stress was increased at the second PP to –142 MPa compared to the NSF value of –113.23 MPa (*p* < 0.001; Table 2). At the second MP, the NI again reduced compressive stress (–104.85 MPa) compared to the NSF (–202 MPa) and the 10°AI (–179.19 MPa) (all *p* values <0.001; Table 2).

TABLE 3 Maximum equivalent tensile stress (or von Mises stress) on the neutral and angled implants after proximal interphalangeal joint arthrodesis on the proximal and middle phalanges of the second, third and fourth toes. *p* value maximum von Mises stress NI versus 10° are <0.001.

Toe (<i>N</i>)	Maximum von Mises stress NI (MPa) average ± SD (minimum –maximum)	Maximum von Mises stress 10° (MPa) average ± SD (minimum –maximum)	<i>p</i> value
At second toe (<i>n</i> = 12 115)	101.12 (19.53 ± 14.81)	227.64 (48.64 ± 35.47)	<0.001
At third toe (<i>n</i> = 7573)	344.54 (59.35 ± 40.47)	403.54 (74.66 ± 51.31)	<0.001
At fourth toe (<i>n</i> = 5103)	101.22 (14.83 ± 11.58)	233.77 (32.61 ± 25.36)	<0.001

Note: *p* < 0.01 (with a 99% confidence interval) was considered statistically significant.

Abbreviations: 10°, 10° angled implant; MPa, megapascal; *N*, total surface represented by the total number of nodes that make up the implant mesh; NI, neutral implant; PIPJA, proximal interphalangeal joint arthrodesis.

At the third PP, the NI again reduced compressive stress (−152 MPa) compared to the NSF (−199 MPa), however, the 10°AI reduced the compressive stress to an even greater extent (−140 MPa) (all *p* values <0.001; Table 2). At the third MP, the NI again reduced compressive stress (−167.01 MPa) compared to the NSF (−308.82 MPa) and the 10°AI (−208.33 MPa) (all *p* values <0.001; Table 2).

At the fourth PP, the NI reduced compressive stress (−18.85 MPa) compared to the NSF (−32.08 MPa) and the 10°AI (−39.90 MPa) (all *p* values <0.001; Table 2). At the fourth MP, the NI also reduced compressive stress (−146.44 MPa) compared to the NSF (−147.39 MPa), however, the 10°AI significantly increased the compressive stress (−288.88 MPa) (all *p* values <0.001; Table 2).

3.1 | Equivalent tensile stress at implants

Table 3 shows the results of the von Mises stress, σ_{vm} ,³⁸ that which can predict the initiation of plastic yielding of metals (such as this alloy) under multiaxial loading conditions. The von Mises stress at the implant was significantly lower when using a NI compared with a 10°AI for all toes analysed (*p* < 0.001). Thus, the risk of implant breakage is lower when using a NI rather than a 10°AI.

In particular, at the third toe, using the 10°AI 10°AI, von Mises stress increased to 403.54 MPa. Since the tensile yield strength was 430 MPa, the value of the von Mises stress for the 10°AI at the third toe was near the point of yielding, increasing the risk of implant fracture.

4 | DISCUSSION

Using FE analysis, the present study assessed the biomechanical efficacy of PIPJA using 10°AI versus NI shape

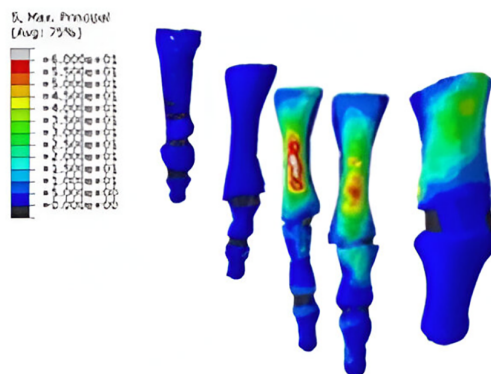
memory intramedullary. In particular, we determined whether these two types of implants could reduce tensile or compressive stresses at the PP and MP joints of the second through fourth toes. We also sought to determine the shape of implant which offers the best biomechanical resistance to breakage and optimum stress distribution at the second through fourth proximal and middle phalanges.

We found that a PIPJA performed on the second toe, using a NI, reduced tensile stress at the PP joint (45.83 MPa) compared to the NSF (59.44 MPa; *p* < 0.001, Table 1). When using the 10°AI, the tensile stress was much higher at PP and MP joints of the same toe, measuring 147.58 MPa and 160.58 MPa, respectively, versus 59.44 MPa and 74.95 MPa at corresponding joints in the NSF (all *p* < 0.001, Table 1). Similar results were found for compressive stresses. The NI reduced compressive stress at the second PP (−65.12 MPa) compared to the NSF (−113.23 MPa) and the 10°AI (−142 MPa) (all *p* < 0.001, Table 2).

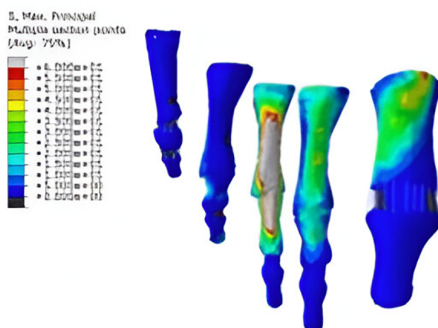
At the third toe, both implants increased the tensile stress at PP and MP joints, compared to the NSF, but the values were increased to a lesser degree using the NI. The increase in tensile stress at the PP and MP was due to the small size of these phalanges, even using the smaller implants. The opposite was found for compressive stresses. Use of the implants lowered the compressive stresses at the third PP and MP joints compared to the NSF (all *p* < 0.001, Table 2).

At the PP of the fourth toe, due to the small size of the PP, the tensile stress from both implants was greater compared with the NSF (43.30 MPa), although the increase in tensile stress occurred to a lesser degree using the NI (150.44 MPa) compared to the 10°AI (250.01 MPa) (all *p* < 0.001). In the MP of the fourth toe, the tensile stress was lowered in the NSF compared to either implant, but to a lesser extent using the NI. The opposite was true for compressive stresses at the fourth toe. Use of

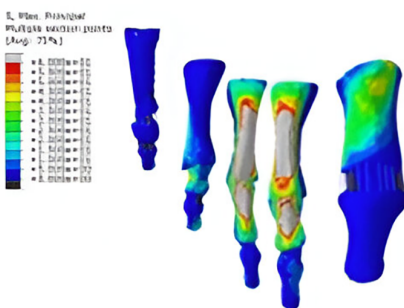
FIGURE 2 Maximum tensile stresses, in megapascals, on the plantar area of the proximal and middle phalanges of the second, third and fourth toes in the two types of implant analysed. U3: Tension stress scale in megapascals. (A) Dorsal view of the maximum compressive stresses withstood by the three phalanges of the second through the fourth toes in the finite element model with no intervention performed. (B) Dorsal view of the maximum tensile stresses withstood by the three phalanges of the second through the fourth toes in the finite element model in which a proximal interphalangeal joint arthrodesis (PIPJA) has been performed using a simulated neutral implant, with the green colour showing lower tensile stresses. (C) Dorsal view of the maximum tensile stresses withstood by the three phalanges of the second through the fourth toes in the finite element model in which a PIPJA has been performed using a simulated 10° angled implant, with the green colour showing lower tensile stress and red/grey indicating higher tensile stress. 10°, 10° angled implant; NI, neutral implant; NSF, non-surgical foot; PIPJA, proximal interphalangeal joint arthrodesis.



(A) - NSF



(B) - Neutral implant



(C) - 10° angled implant

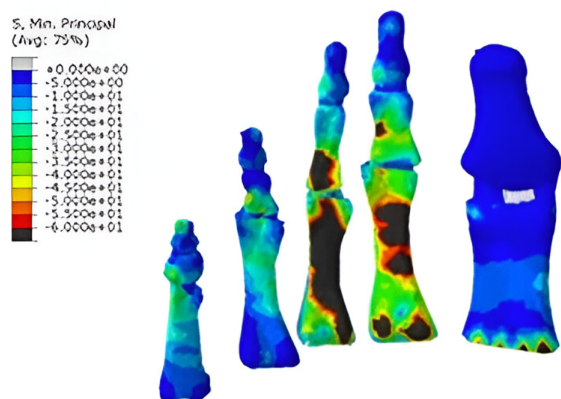
the NI slightly lowered the compressive stress at both the fourth PP (−18.85 MPa) and the fourth MP (−146.44 MPa) compared to the NSF where the compressive stresses measured −32.08 MPa and −147.39 MPa, respectively (all $p < 0.001$, Table 2).

The fact that tensile stresses primarily affected the dorsal area (Figure 2) whereas compressive stresses affected the plantar area (Figure 3) confirmed that a state of flexion existed in the phalanges.

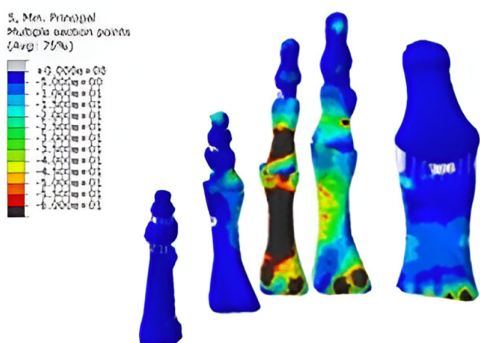
Comparison of the tensile stress distributions showed that the loaded area was different for PIPJA when using a NI versus 10°AI. The proximal and middle phalanges were loaded on all their surfaces using the 10°AI, whereas for the NI, phalanges

were less loaded (Figure 4). Similar results were obtained when comparing compressive stresses. Both PP and MP joints at the second through fourth toes were loaded on all their surfaces using the 10°AI, whereas for the NI, the phalanges were less loaded.

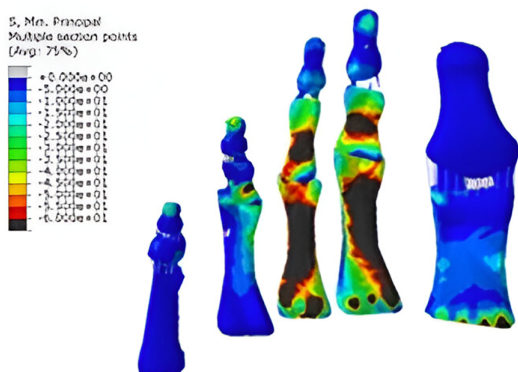
The von Mises stresses within the implants were also significantly lower when using the NI versus 10°AI for all three toes ($p < 0.001$, Table 3). The von Mises stress distribution results showed that the NI had values that were all below the elastic limit of the implant material (430 MPa). In contrast, the 10°AI had values close to the elastic limit at the third toe (403.54) which could result in implant failure.



(A) - NSF



(B) - Neutral implant



(C) - 10° angled implant

FIGURE 3 Maximum compressive stresses, in megapascals, on the plantar area of the proximal and middle phalanges of the second, third and fourth toes in the two implant types analysed. U3: Compression stress scale in megapascals. (A) Plantar view of the maximum compressive stresses withstood by the three phalanges of the second through the fourth toes in the finite element model with no intervention performed. (B) Plantar view of the maximum compressive stresses withstood by the three phalanges of the second through the fourth toes in the finite element model in which a proximal interphalangeal joint arthrodesis (PIPJA) has been performed using a simulated neutral implant, with the green colour showing lower compressive stresses. (C) Plantar view of the maximum compressive stresses withstood by the three phalanges of the second through the fourth toes in the finite element model in which a PIPJA has been performed using a simulated 10° angled implant, with the green colour showing lower compressive stress and red/black colour indicating higher compressive stress. NSF, non-surgical foot; NI, neutral implant; 10°, 10° angled implant; PIPJA, proximal interphalangeal joint arthrodesis.

In view of the above findings, use of the 10° AI is not recommended to alleviate the problem of HT. Although kinematics alleviates the problem, significant increases in tension can cause pain in the patient after surgery and could lead to implant breakage due to the shape of the implant. In the 10° AI, the 10° angle promotes stress concentration around the angularity. We, therefore, recommend the use of the largest NI when performing a PIPJA of the second toe due to greater reduction in tensile stress at the PP and MP joints compared to the 10° AI. We do not recommend the use of the NI when performing a PIPJA of the third and fourth toes as it causes significantly increased tensile stresses at the PP and MP joints

of the third toe and MP joint of the fourth toe which could result in implant fracture. In the surgeon's opinion, however, if PIPJA is needed, we recommend the use of the smallest NI for third and fourth toes to avoid implant failure.

Our study had several limitations. In this work, only the push-off phase of the gait cycle was reproduced since it is the most critical gait position. A complete simulation of the entire cycle, however, would lead to a better understanding of the biomechanics at the phalanges in future investigations. All materials were considered elastic and linear because calculus were done under hypothesis of small displacements and small strains. Finally, the loads

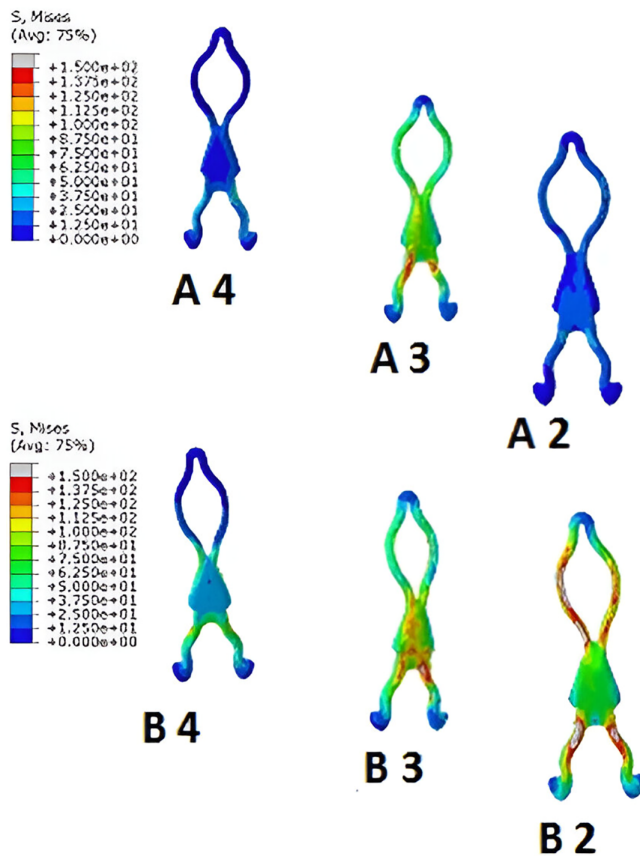


FIGURE 4 Maximum von Mises stress at the implant after proximal interphalangeal joint arthrodesis at second, third and fourth toes for the two implant types analysed. A2, A3 and A4: Neutral implant at second, third and fourth toes, respectively. B2, B3 and B4: Angled implant at second, third and fourth toes, respectively. With the blue colour depicting lower von Mises stress and red/grey colour indicating higher von Mises stress. A, neutral implant; B, 10° angled implant; 2, second toe; 3, third toe; 4, fourth toe.

considered were based on a male weighing 60 kg. If this value was modified, numerical results would be different but, qualitatively, they would be analogous.

5 | CONCLUSIONS

This study does not recommend performing a PIPJA using the 10° AI to alleviate the problem of HT, primarily at the second toe, because significant increases in tensile stress after surgery could lead to implant failure. In light of our results, the NI reduced both tensile and compressive stresses at the PP and MP joints of the second toe compared to the 10° AI. Therefore, we recommend the use of the largest NI when performing a PIPJA of the second toe.

ACKNOWLEDGEMENTS

The authors gratefully acknowledge the support of the project DPI2013-44987-R belonging to the Economy and Competitiveness Ministry and Funding for open access charge: Universidade da Coruña/CISUG.

CONFLICT OF INTEREST STATEMENT

The author declares no conflicts of interest.

DATA AVAILABILITY STATEMENT

The dataset supporting the conclusions of this article is available upon request to daniellopez@udc.es in the Research, Health and Podiatry Group. Department of Health Sciences. Faculty of Nursing and Podiatry. Industrial Campus of Ferrol. Universidade da Coruña.

ORCID

Daniel López-López  <https://orcid.org/0000-0002-9818-6290>

REFERENCES

1. Cyphers SM, Feiwell E, Feiwell E, Feiwell E. Review of the Girdlestone-Taylor procedure for clawtoes in myelodysplasia. *Foot Ankle*. 1988;8(5):229-233.
2. Menz HB, Lord SR. The contribution of foot problems to mobility impairment and falls in community-dwelling older people. *J Am Geriatr Soc*. 2001;49(12):1651-1656.
3. López-López D, Martínez-Vázquez M, Losa-Iglesias ME, et al. Foot health-related quality of life among elderly with and without lesser toe deformities: a case-control study. *Patient Prefer Adherence*. 2018;12:251-255.
4. Gallentine JW, DeOrio JK. Removal of the second toe for severe hammertoe deformity in elderly patients. *Foot Ankle Int*. 2005;26(5):353-358.
5. Coughlin MJ. Lesser toe abnormalities. *Instr Course Lect*. 2003; 52:421-444.
6. Yu GV, Judge MS, Hudson JR, Seidelmann FE. Predislocation syndrome. Progressive subluxation/dislocation of the lesser metatarsophalangeal joint. *J Am Podiatr Med Assoc*. 2002;92(4): 182-199.
7. Lamm BM, Ribeiro CE, Vlahovic TC, Fiorilli A, Bauer GR, Hillstrom HJ. Lesser proximal interphalangeal joint arthrodesis: a retrospective analysis of the peg-in-hole and end-to-end procedures. *J Am Podiatr Med Assoc*. 2001;91(7):331-336.
8. McGlamry ED, Southerland JT, Vickers D, Boberg JS. McGlamry's comprehensive textbook of foot and ankle surgery. 2002.
9. Miller SJ. Hammer toe correction by arthrodesis of the proximal interphalangeal joint using a cortical bone allograft pin. *J Am Podiatr Med Assoc*. 2002;92(10):563-569.
10. Schlefman BS, Fenton CF, McGlamry ED. Peg in hole arthrodesis. *J Am Podiatry Assoc*. 1983;73(4):187-195.
11. Patton GW, Shaffer MW, Kostakos DP. Absorbable pin: a new method of fixation for digital arthrodesis. *J Foot Surg*. 1990; 29(2):122-127.

12. Reece AT, Stone MH, Young AB. Toe fusion using Kirschner wire. A study of the postoperative infection rate and related problems. *J R Coll Surg Edinb.* 1987;32(3):158-159.
13. Caterini R, Farsetti P, Tarantino U, Potenza V, Ippolito E. Arthrodesis of the toe joints with an intramedullary cannulated screw for correction of hammertoe deformity. *Foot Ankle Int.* 2004;25(4):256-261.
14. Edwards WHB, Beischer AD. Interphalangeal joint arthrodesis of the lesser toes. *Foot Ankle Clin.* 2002;7(1):43-48.
15. Imhaeuser G. Operation of hammer toes and claw toes, and treatment of unfavourable results (author's transl). *Z Orthop Ihre Grenzgeb.* 1979;117(2):179-184.
16. Konkel KF, Menger AG, Retzlaff SA. Hammer toe correction using an absorbable intramedullary pin. *Foot Ankle Int.* 2007;28(8):916-920.
17. Ohm OW, McDonell M, Vetter WA. Digital arthrodesis: an alternate method for correction of hammer toe deformity. *J Foot Surg.* 1990;29(3):207-211.
18. O'Kane C, Kilmartin T. Review of proximal interphalangeal joint excisional arthroplasty for the correction of second hammer toe deformity in 100 cases. *Foot Ankle Int.* 2005;26(4):320-325.
19. Shaw AH, Alvarez G. The use of digital implants for the correction of hammer toe deformity and their potential complications and management. *J Foot Surg.* 1992;31(1):63-74.
20. Yu GV, Vincent AL, Khoury WE, Schinke TL. Techniques of digital arthrodesis: revisiting the old and discovering the new. *Clin Podiatr Med Surg.* 2004;21(1):17-50.
21. Angirasa AK, Barrett MJ, Silvester D. SmartToe[®] implant compared with Kirschner wire fixation for hammer digit corrective surgery: a review of 28 patients. *J Foot Ankle Surg.* 2012;51(6):711-713.
22. Delmi M. *Hammer Toe Surgical Correction.* Memometal Inc; 2012.
23. Boyer ML, DeOrio JK. Transfer of the flexor digitorum longus for the correction of lesser-toe deformities. *Foot Ankle Int.* 2007;28(4):422-430.
24. Bandak FA, Tannous RE, Toridis T. On the development of an osseo-ligamentous finite element model of the human ankle joint. *Int J Solids Struct.* 2001;38(10-13):1681-1697.
25. Cheung JTM, Zhang M, Leung AKL, Fan YB. Three-dimensional finite element analysis of the foot during standing – a material sensitivity study. *J Biomech.* 2005;38(5):1045-1054.
26. Gefen A. Stress analysis of the standing foot following surgical plantar fascia release. *J Biomech.* 2002;35(5):629-637.
27. Gefen A, Megido-Ravid M, Itzhak Y, Arcan M. Biomechanical analysis of the three-dimensional foot structure during gait: a basic tool for clinical applications. *J Biomech Eng.* 2000;122(6):630-639.
28. García-Aznar JM, Kuiper JH, Gómez-Benito MJ, Doblare M, Richardson JB. Computational simulation of fracture healing: influence of interfragmentary movement on the callus growth. *J Biomech.* 2006;40(7):1467-1476.
29. García-Aznar JM, Bayod J, Rosas A, et al. Load transfer mechanism for different metatarsal geometries: a finite element study. *J Biomech Eng.* 2009;131(2):021011.
30. García-González A, Bayod J, Prados-Frutos JC, et al. Finite-element simulation of flexor digitorum longus or flexor digitorum brevis tendon transfer for the treatment of claw toe deformity. *J Biomech.* 2009;42(11):1697-1704.
31. Bayod J, Losa-Iglesias M, De Bengoa-Vallejo RB, Prados-Frutos JC, Jules KT, Doblare M. Advantages and drawbacks of proximal interphalangeal joint fusion versus flexor tendon transfer in the correction of hammer and claw toe deformity: A finite-element study. *J Biomech Eng.* 2010;132(5):051002.
32. Marks RM. Anatomy and pathophysiology of lesser toe deformities. *Lesser Toe Deformities.* WB Saunders; 1987:78.
33. Bayod J, Becerro-de-Bengoa-Vallejo R, Losa-Iglesias ME, Doblare M. Mechanical stress redistribution in the calcaneus after autologous bone harvesting. *J Biomech.* 2012;45(7):1219-1226.
34. Gómez-Benito MJ, Fornells P, García-Aznar JM, Seral B, Seral-Iñigo F, Doblare M. Computational comparison of reamed versus unreamed intramedullary tibial nails. *J Orthop Res.* 2007;25(2):191-200.
35. Sebastian H, Datta B, Maffulli N, Neil M, Walsh WR. Mechanical properties of reconstructed achilles tendon with transfer of peroneus brevis or flexor hallucis longus tendon. *J Foot Ankle Surg.* 2007;46(6):424-428.
36. Murphy W, Black J, Hastings G. *Handbook of Biomaterial Properties.* 2nd ed. Springer; 2016:1-676.
37. Liu Y. The superelastic anisotropy in a NiTi shape memory alloy thin sheet. *Acta Mater.* 2015;95:411-427.
38. Zhou H, Xu D, Quan W, Ugbolue UC, Zhou Z, Gu Y. Can the entire function of the foot be concentrated in the forefoot area during the running stance phase? A finite element study of different shoe soles. *J Hum Kinet.* 2024;92:5-17.
39. Zhang Q, Zhang Y, Chon TE, Baker JS, Gu Y. Analysis of stress and stabilization in adolescent with osteoporotic idiopathic scoliosis: finite element method. *Comput Methods Biomech Biomed Engin.* 2023;26(1):12-24.
40. Xiang L, Mei Q, Wang A, Shim V, Fernandez J, Gu Y. Evaluating function in the hallux valgus foot following a 12-week minimalist footwear intervention: a pilot computational analysis. *J Biomech.* 2022;132:110941.
41. Seireg A, Arvikar RJ. The prediction of muscular load sharing and joint forces in the lower extremities during walking. *J Biomech.* 1975;8(2):89-102.
42. Kitaoka HB, Luo ZP, An KN. Three-dimensional analysis of normal ankle and foot mobility. *Am J Sports Med.* 1997;25(2):238-242.
43. Stauffer RN, Chao EYS, Brewster RC. Force and motion analysis of the normal, diseased, and prosthetic ankle joint. *Clin Orthop Relat Res.* 1977;127:189-196.

How to cite this article: Bayod-López J, Becerro-de-Bengoa-Vallejo R, Prados-Frutos JC, Losa-Iglesias M, López-López D, Prados-Privado M. Influence of the biomechanical evaluation of rupture using two shapes of same intramedullary implant after proximal interphalangeal joint arthrodesis to correct the claw/hammer pathology: A finite element study. *Int Wound J.* 2024;21(8):e70014. doi:[10.1111/iwj.70014](https://doi.org/10.1111/iwj.70014)